HHS Public Access

Author manuscript

Bone. Author manuscript; available in PMC 2018 April 01.

Published in final edited form as:

Bone. 2017 April ; 97: 243–251. doi:10.1016/j.bone.2017.01.015.

Assessment of collagen quality associated with non-enzymatic cross-links in human bone using Fourier-transform infrared imaging

F.N. Schmidt[a], **E.A. Zimmermann**[a], **G.M. Campbell**[b], **G.E. Sroga**[c], **K. Püschel**[d], **M. Amling**[a], **S. Y. Tang**[e], **D. Vashishth**[c], and **B. Busse**[a,*]

[a]Department of Osteology and Biomechanics, University Medical Center, 22529 Hamburg, Germany

[b]Institute of Biomechanics, Hamburg University of Technology, 21073 Hamburg Germany

[c]Department of Biomedical Engineering, Center for Biotechnology and Interdisciplinary Studies, Rensselaer Polytechnic Institute, Troy NY 12180, USA

[d]Department of Forensic Medicine, University Medical Center, 22529 Hamburg, Germany

[e]Department of Orthopaedics, Washington University in St. Louis, St. Louis, MO, USA

Abstract

Aging and many disease conditions, most notably diabetes, are associated with the accumulation of non-enzymatic cross-links in the bone matrix. The non-enzymatic crosslinks, also known as advanced glycation end products (AGEs), occur at the collagen tissue level, where they are associated with reduced plasticity and increased fracture risk. In this study, Fourier-transform infrared (FTIR) imaging was used to detect spectroscopic changes associated with the formation of non-enzymatic cross-links in human bone collagen. Here, the non-enzymatic cross-link profile was investigated in one cohort with an *in vitro* ribose treatment as well as another cohort with an *in vivo* bisphosphonate treatment. With FTIR imaging, the two-dimensional (2D) spatial distribution of collagen quality associated with non-enzymatic cross-links was measured through the area ratio of the 1678/1692 cm^{-1} subbands within the amide I peak, termed the non-enzymatic crosslink-ratio (NE-xLR). The NE-xLR increased by 35% in the ribation treatment group in comparison to controls ($p < 0.005$), with interstitial bone tissue being more susceptible to the formation of non-enzymatic cross-links. Ultra high performance liquid chromatography, fluorescence microscopy, and fluorometric assay confirm a correlation between the non-enzymatic cross-link content and the NE-xLR ratio in the control and ribated groups. High resolution FTIR imaging of the 2D bone microstructure revealed enhanced accumulation of non-enzymatic cross-links in bone regions with higher tissue age (i.e., interstitial bone). This non-enzymatic cross-link ratio (NE-xLR) enables researchers to study not only the overall content of AGEs in the bone but

*Corresponding author: Björn Busse, Ph.D., Department of Osteology and Biomechanics, University Medical Center, Lottestraβe 55a, 22529 Hamburg, Germany, Tel.: (+49) 40 7410 - 56687, Fax: (+49) 40 7410 – 40400, b.busse@uke.uni-hamburg.de.

also its spatial distribution, which varies with skeletal aging and diabetes mellitus and provides an additional measure of bone's propensity to fracture.

Keywords

advanced glycation end products; non-enzymatic cross-links; Fourier transform infrared spectroscopy; collagen; bisphosphonates; bone quality

1 Introduction

Human bone resists deformation and fracture through its hierarchical structure, which shields growing cracks at large length-scales and generates plasticity at small length-scales [1]. Alterations to the bone structure in disease states can alter the mechanical properties and ultimately increase the risk of bone fracture, such as in diabetes mellitus, aging, and vitamin D deficiency [2–4]. In the bone structure, non-enzymatic cross-links are of particular interest because they are associated with many disease states and increased fracture risk [4–7]. Here, we investigate non-enzymatic cross-links in bone using Fourier-transform infrared (FTIR) imaging, which is a non-destructive spectroscopic method to detect compositional changes at a high spatial resolution.

Cross-links form at the nano-level in human bone, where fibrils are composed of collagen molecules embedded with mineral platelets [8]. At this scale, cross-links form between collagen molecules and between fibrils either enzymatically or non-enzymatically. *Enzymatic cross-links* stabilize the arrangement of collagen and fibrils in new bone material, where reducible enzymatic cross-links form between collagen molecules and eventually mature into irreducible cross-links between fibrils [8,9]. These cross-links can only form at specific points along the collagen molecule so their number is greatly limited. Conversely, *non-enzymatic cross-links* form at any point along the collagen molecule to connect either collagen molecules or fibrils [9]. Non-enzymatic cross-links are commonly referred to as advanced glycation end-products (AGEs) because they form through a glucose-mediated reaction, which may be highly influenced by oxidative stresses [6,10]. There are many different non-enzymatic cross-links, but the most commonly studied are the fluorescent crosslink pentosidine [11] and carboxymethly-lysine (CML) [12].

Non-enzymatic cross-links in bone are of high interest because they are associated with reduced mechanical performance [4,7,12–15]. Indeed, bone's stiffness and strength originate from deformation of mineralized collagen fibrils [1]. Non-enzymatic cross-links reduce the mechanical properties by restricting fibrillar deformation, which is an essential plasticity mechanism in bone at the fibrillar length-scale. Indeed, reductions in fibrillar strain, post-yield strain energy and post-yield strain are associated with higher contents of non-enzymatic cross-links [4,7,16]. Thus, non-enzymatic cross-links may contribute to increased fracture risk when they accumulate during diabetes [13], aging [6], irradiation [16], and osteoporosis [17– 19]. In addition, *in vivo* animal experiments have shown that high doses of bisphosphonate administration, which is a common treatment for osteoporosis, lead to increased levels of non-enzymatic cross-links in canine bone [20,21].

Currently, non-enzymatic cross-links are measured using high-performance liquid chromatography (HPLC) [22–24] or fluorometric assays [7,21]. While these methods provide direct quantitative information on the amount of non-enzymatic cross-links, they do have certain limitations. In particular, the measurements do not provide spatial information on the distribution of non-enzymatic cross-links within the microstructure. In addition, the sample preparation is time-consuming and requires destruction of the sample.

FTIR is a spectroscopy method commonly used to characterize the composition of bone tissue [25–29]. Infrared radiation is absorbed by the sample at wavenumbers that are characteristic of the molecular composition. In bone, FTIR detects amide vibrations from the collagen as well as phosphate vibrations from the mineral component (Figure 1a). Consequently, FTIR has been used to establish the following parameters to describe bone material quality: mineral-to-matrix ratio, crystallinity (*i.e.,* mineral crystal size), carbonate-to-phosphate ratio (*i.e.,* the maturity of the mineral), and collagen maturity (*i.e.,* the level of enzymatic cross-linking) [29]. As sample preparation for FTIR analysis preserves the structure and is comparable to routine histological preparations, FTIR imaging allows investigation of consecutive matching regions of interest highlighted by either specific histological stains or pseudo-colored compositional spectroscopic maps. Using FTIR to measure the content of crosslinks in the collagenous network has been previously explored on collagen I gels and tail tendon collagen I extracts [30,31]. These studies found a correlation between the non-enzymatic cross-link profile and signals from the carbohydrate (1100 – 900 cm^{-1}) and amide I peaks; however, in a complex tissue such as bone, mineral and proteoglycan components are also present in this region of bone's FTIR spectrum [32]. Therefore, complex biological tissues that contain more than just type I collagen fibrils require additional extensive data analysis.

Here, we investigate changes in collagen quality associated with non-enzymatic cross-linking in human bone using FTIR imaging. First, the FTIR spectrum of the non-enzymatic collagen cross-links, pentosidine, was used to identify the spectral regions of interest that absorb infrared radiation linked to non-enzymatic collagen cross-links. Next, we performed *in vitro* control and ribation treatments on a set of human bone samples to increase the non-enzymatic cross-link content. Then, the increase in non-enzymatic cross-links in the ribation treatment vs. control groups was measured with four methods: ultra high-performance liquid chromatography (UPLC), fluorometric assay, fluorescence microscopy and FTIR imaging. FTIR imaging and the fluorescence microscopy were further used with a cohort of human iliac crest biopsies taken from patients suffering from osteoporosis as well as following anti-resorptive bisphosphonate (BP) treatment.

2 Materials and Methods

2.1 Pentosidine standard

2.1.1 FTIR measurement of pentosidine standard—Pentosidine is the non-enzymatic cross-link most commonly used to quantify the amount of non-enzymatic cross-links in bone. Here, a pentosidine standard was used to find the infrared absorptions associated with non-enzymatic cross-links. A standard containing only pentosidine was acquired in crystalline form (Biomol GmbH, Germany). The crystallized sample was

dissolved in distilled water on a low-e microscope slide (Kevely Technologies, Chesterland, Ohio, USA). After evaporation of the water, the FTIR spectra were collected with a FTIR Spotlight 400 (PerkinElmer, Waltham, Massachusetts, USA), attached to an FTIR Spectrometer Frontier (PerkinElmer, Waltham, Massachusetts, USA). The spectra were acquired in a reflective transmittance mode over a spectral range of 4000 to 570 cm^{-1} at a resolution of 2 cm^{-1} and with 16 scans per pixel. From the FTIR scan of pentosidine, the characteristic peaks of the standard were found using Spectrum software version 10.08.09 (PerkinElmer, Waltham, Massachusetts, USA).

2.2 Investigation of non-enzymatic cross-links with FTIR: ribose-treated bone

2.2.1 Materials—Healthy human femoral bone from organ donors was acquired at autopsy. The cortical bone samples were taken from the mid-diaphyseal regions of the femur from individuals younger than 14 years of age to limit age-related accumulation of non-enzymatic cross-links (n = 8) [6]. All donors died by non-bone-related diseases or accidents. None of the donors exhibited metabolic bone diseases. The study was approved by the Ethics Committee of the Hamburg Chamber of Physicians.

From each donor, sections of cortical bone from the mid-diaphysis were cut using a low speed saw (EXAKT Advanced Technologies GmbH, Norderstedt, Germany). The bone sections were approximately 6 × 3 mm in the transverse orientation and included the whole cortical thickness (*i.e.,* periosteum to endosteum). Two consecutive sections of bone were taken from each donor at the same position and either treated with a control protocol or with a ribation treatment to increase the non-enzymatic cross-link content. A control on which quadrant the specimen was taken was not possible. Control specimens were placed in a solution consisting of 1-ml toluene, 1-ml chloroform, 50-mg gentamycin and filled up to 100 ml with Hanks buffered salt solution (HBSS). Toluene, chloroform and gentamycin were added to prevent bacterial growth. Non-enzymatic cross-links were induced *in vitro* with ribation, according to the methods of Vashishth *et al.* [7]. The ribation solution was identical to the control solution but also contained 10 g of D-ribose. The control and ribose-treated specimens were immersed in their respective solution in a single 15-ml polypropylene tube and incubated for four weeks at 37°C. After treatment, each sample was cut in half using a low-speed saw. The first half was prepared for FTIR, fluorescence microscopy and UPLC and the second half was used in a fluorometric assay. All specimens were washed extensively with Hank's buffered salt solution (HBSS) after the embedding process to ensure that no spectral artifacts from the incubation solution were present.

2.2.2 FTIR sample preparation—Following treatment, the control and ribated samples were dehydrated in an increasing alcohol series and then infiltrated with polymethylmethacrylate (PMMA) (Merck, Darmstadt, Germany). The PMMA-embedded sections were then cut with a microtome (Reichert Jung, Germany) to a thickness of 4 μm. Then, the sections were soaking in EDTA (20% in distilled water) for two minutes for demineralization. Afterwards, the sections were cleaned extensively with distilled water and then transferred to a low-e microscope slide (Kevley Technologies, Chesterland, Ohio, USA) for FTIR analysis. Microtomed sections that had not been sufficiently rinsed with distilled

water were easily identifiable with a peak in the FTIR spectra at 1596 cm^{-1} and were not included in the analysis.

2.2.3 FTIR imaging—FTIR spectroscopic measurements of the human bone samples were carried out using the FTIR microscope. The FTIR imaging microscope collects spectra over an area to create an image, where the pixels represent individual spectra. For every specimen, spectra were acquired at a 6.25-μm step size (*i.e.,* pixel size) over a cortical area of 250 × 250 $μm^2$. The spectra were acquired in reflective transmittance mode over a spectral range of 4000 to 570 cm^{-1} wave numbers at a resolution of 2 cm^{-1} and with 16 scans per pixel. An automated atmospheric correction (SpectrumImage R V 1.7.1.0401 by PerkinElmer, Waltham, MA, USA) and a background subtraction on the measured samples ensured no influence of the atmosphere due to water vapor, *etc.*

2.2.4 FTIR data analysis—Each FTIR image contained roughly 1600 spectra that were post-processed using a customized MATLAB routine. For each spectra, linear baseline correction was performed and the PMMA signal was subtracted [33]. Pixels containing a high amount of PMMA were taken out of the evaluation to prevent edge effects at the border between PMMA and bone.

The amide I band possesses structural information about the collagen matrix and is also the location of the strongest peaks for the non-enzymatic cross-link pentosidine (see Figure 1b). Therefore, the amide I peak was targeted (1710 - 1600 cm^{-1}) to find a subband ratio to quantify the effect of changes in the non-enzymatic cross-link content on the bone matrix. First, the positions of the underlying subbands in the amide I peak were determined using the second derivative of the spectrum for every measured spectrum (i.e., pixel). All subband positions were mapped in a histogram to get an adequate indication of the underlying peak positions following their frequency. Based on this second derivative analysis, seven Gaussian peaks were chosen to fit the amide I band: 1702, 1692, 1678, 1661, 1645, 1630, and 1610 cm^{-1}. These peaks were chosen according to the second derivative of the average spectrum of the specimens and known peak-positions from the literature [34–37].

Once the appropriate subbands had been chosen, each spectra in the FTIR maps was fit with these exact subbands. The difference between the peak fitted model and real spectrum was < 0.6 % in absorbance intensity at every wavelength. After peak fitting, the area ratio of the 1678 and 1692 cm^{-1} peaks was calculated and an image was produced, where the pixel color corresponds to the value of the ratio at the specific measurement position. An average of all valid data points (max. 1600) for every picture was done to calculate the average value for each ratio per specimen.

In addition, other established FTIR parameters were measured from the FTIR spectra. From the analysis of the amide I subbands, the matrix maturity ratio (1661 and 1692 cm^{-1}) and the enzymatic cross-link ratio (using the rate 1661/1678 cm^{-1} ratio) were measured [29,38]. Furthermore, a second measurement in attenuated total reflection-mode (ATR) was done on the remaining mineralized specimen before UPLC analysis. The areas under the curve of the amide I peak, the phosphate peak (1140 – 900 cm^{-1}) and the carbohydrate peak (890 - 850

cm^{-1}) were integrated to measure the carbonate-to-phosphate ratio and the mineral-to-matrix ratio [29].

2.2.5 Fluorometric Assays—A fluorometric assay was performed to evaluate the extent of non-enzymatic collagen cross-linking in the bone samples using a previously established method [7, 17]. After the control or ribation treatment, the bone was demineralized using EDTA and then hydrolyzed using 6 N HCl (24 h, 110°C). The non-enzymatic cross-link content was determined using fluorescence readings taken using a micro plate reader at the excitation wavelength of 370 nm and emission wavelength of 440 nm. These readings were standardized to a quinine-sulfate standard and then normalized to the amount of collagen present in each bone sample. The amount of collagen for each sample was determined based on the amount of hydroxyproline, the latter being determined using a chloramine-T colorimetric assay that recorded the absorbance of the hydrolysates against a commercially available hydroxyproline standard at the wavelength of 585 nm [39].

2.2.6 Fluorescence Microscopy—Fluorescence microscopy was performed on all specimens (control, D-ribose treated, osteoporosis cases and bisphosphonate-treated cases) using histological sections. Sections were cut to a 4-μm thickness and then demineralized in an EDTA solution (17%) for 3 minutes. After demineralization, all specimens were washed extensively with distilled water, stretched with 90% Ethanol and covered using fluorescence mounting medium (Dako, Glostrup, Denmark). The slides were then imaged using a fluorescence microscope (Nikon Eclipse 80i) at 360-nm excitation with a 470 ± 40nm emission filter with an exposure time of 0.25 seconds. For every sample, the fluorescence intensity was calculated at three random locations (ImageJ) and the peak of the intensity histogram corresponding to the fluorescence was recorded.

2.2.7 Ultra-high pressure liquid chromatography—Acid hydrolysis of bone samples was performed in 6N HCl (100 μl/mg bone) at 110°C for 20 hrs. After completion of the hydrolysis, the hydrolysates were centrifuged. Each supernatant was transferred to a clean tube and used directly for the assays or stored at −80°C as needed. Determination of pentosidine was performed using ultra-high pressure liquid chromatography (UPLC) [23,24].

2.3 Investigation of non-enzymatic cross-links with FTIR: osteoporosis cases and bisphosphonate treatment

2.3.1 Materials—FTIR imaging was furthermore used to image the non-enzymatic cross-linking distribution in human osteoporotic trabecular bone and after bisphosphonate treatment. Here, iliac crest biopsies were acquired from a cohort of 14 individuals (10 male, 4 female) before and after administration of a third generation bisphosphonate, which was prescribed along with adequate calcium and vitamin D supplementation. At the time of the first biopsies the mean age of the individuals was 51.35 ± 12.19 years [40]. The average bisphosphonate treatment period was 55.71 ± 22.37 months. Directly after the biopsies were taken, they were fixed in formaldehyde for 48 hours, dehydrated in an increasing alcohol series and then infiltrated with polymethylmethacrylate. The specimens were then stored in a dark room at room temperature. At the time of FTIR imaging, the specimens were sectioned,

demineralized and the areas containing trabecular bone were analyzed with the FTIR, as described above.

2.4 Statistics

Statistics were performed using SPSS 22 (IBM, Armonk, New York, USA). For each map, the average and standard deviation for the points containing bone were calculated. Groups were analyzed for normality using the Kolmogorov-Smirnov-Test. In the case of a non-normal distribution, a Mann-Whitney U test was carried out with a significance level of $\alpha = 0.05$. At normal distribution, a paired t-test ($\alpha = 0.05$) was performed. In case of use of Mann-Whitney-U test, the usage is pointed out in the results section. Ribose-treated samples were all obtained from the same skeletal site and analyzed by means of a paired t-test. Due to contra-lateral biopsy withdrawal, an unpaired t-test was performed on this cohort of samples.

To compare the FTIR results to established measurements of cross-link content (i.e., UPLC, fluorometric assay, fluorescent imaging), a Pearson correlation was calculated and a regression was performed including the calculation of an r^2. Only significant ($p < 0.05$) correlations were further processed to achieve a regression. For a regression model an ANOVA of control and D-ribose-treated bone was done and considered to be significant at a p-value < 0.05. Coefficients of the regression models were considered to be significant at a p-value < 0.05.

ANOVA for a comparison of control, D-Ribose-treated, osteoporotic bone and BP-treated osteoporosis cases was done and considered to be significant at a p-value < 0.05. As post-hoc analysis, a Tukey-B test was performed and groups allocated to different subsets were considered to be significantly different to each other at an $\alpha = 0.05$ level.

3 Results

3.1 Pentosidine spectrum

The FTIR spectrum for pure pentosidine was measured and compared to the FTIR spectrum of human bone (Figure 1). The pentosidine sample has several well-defined peaks that overlap with the amide I (1720 – 1600 cm^{-1}) and phosphate bands (1200 – 900 cm^{-1}) in bone. The subbands of the pentosidine peak within the amide I region were located at 1678, 1654, and 1602 cm^{-1} and within the phosphate band at 1202 and 1136 cm^{-1}. Here, the amide I subbands were set as targets for the detection of non-enzymatic cross-links with FTIR.

3.2 Investigation of non-enzymatic cross-links with FTIR: control vs. ribose-treated bone

FTIR imaging was performed on human cortical bone from a juvenile cohort, where consecutive tissue sections from each case were given either a control or ribose treatment, which is a common method to induce non-enzymatic cross-links *in vitro* [7]. Following treatment, the control-treated sections had a light white-yellow color, which is characteristic of young, control tissue (see inset of Figure 2a), while the ribose-treated sections had a darker yellow-orange color (see inset of Figure 2b), which is characteristic of older tissue or tissue with a high non-enzymatic cross-link content [7].

FTIR imaging was used to collect FTIR spectra over a 2D area of the cross-section. From the spectra, the amide I (1720 – 1600 cm^{-1}) subbands were fit with Gaussian peaks and peak area ratios were calculated. The peak area ratio that exhibited a significant difference between the control and ribation treatment groups was formed from the area ratio of the 1678 and 1692 cm^{-1} subbands of the amide I peak. Figure 2 shows a representative fitting of the amide I peak's subbands from the spectra of control and ribose-treated samples with the peaks of interest shaded. Here, we refer to the area ratio of 1678 / 1692 cm^{-1} subbands as the non-enzymatic crosslink-ratio (NE-xLR). The average value of the NE-xLR was 35% higher in the ribation treatment group (Figure 3a) (control: NE-xLR = 8.79 ± 1.65, ribation: NE-xLR = 11.95 ± 1.55, $p < 0.005$ in a paired t-test). The distribution of the NE-xLR ratio across the bone microstructure can be seen in the FTIR images (Figure 3b, c), which were acquired at step sizes of 6.25 μm over a 250 × 250 $μm^2$ cortical area. In the FTIR maps of the NE-xLR (Figure 3b, c), the interstitial bone (older tissue) shows higher values for the NE-xLR. Osteons are evident as round or oval structures with a lower NE-xLR compared to the surrounding interstitial bone material (Figure 3).

A UPLC analysis, fluorescence microscopy, and a fluorometric assay were performed on the control and ribose-treated samples to confirm the higher non-enzymatic cross-link content measured by FTIR in the ribated group. Here, the UPLC analysis measured the content of the non-enzymatic cross-link, pentosidine. The results of the UPLC analysis (Figure 4a) show a 120 times higher average pentosidine content in the ribated group (control: nmol PEN/μmol Collagen = 5.23 ± 4.23, ribated: nmol PEN/μmol Collagen = 636.21 ± 592.81, $p < 0.01$). Additionally, a Pearson correlation analysis revealed a significant correlation between the UPLC results and the NE-xLR from the FTIR analysis with a correlation coefficient of $r = 0.642$, ($p < 0.01$), see Figure 4b.

Fluorescence microscopy measures fluorescence from the fluorescent non-enzymatic cross-links in bone. The peak fluorescence emitted from the samples at an intensity of 360 nm was measured with fluorescence microscopy. The fluorescence was 470% higher in the ribated samples in comparison to controls (Figure 4c) (control: peak fluorescence = 24.08 ± 5.54, ribation: peak fluorescence = 113.13 ± 7.26, $p < 0.00001$). A Pearson correlation between the peak fluorescence and the NE-xLR showed a significant correlation ($p < 0.005$) with $r = 0.713$ at an $r^2 = 0.508$ and a resulting regression equation of $y = 0.0345 x + 8.0064$ (Figure 4d). Representative fluorescence microscopy images shown in Figure 4e, f show the dramatic difference in fluorescence from non-enzymatic cross-links between the control and ribated samples.

The non-enzymatic cross-link content in the control and ribated groups was also measured with a fluorometric assay. Here, the results of the fluorometric assay show a tendency towards a higher non-enzymatic cross-link content in the ribation group (Figure 4g) but did not reach significance (control: non-enzymatic cross-link content = 4.97 ± 1.87, ribation: non-enzymatic cross-link content = 8.4 ± 4.16 ng quinine/mg collagen, $p = 0.067$). However, a Pearson correlation between the results of the FTIR analysis and the fluorometric assay revealed a significant ($p < 0.005$) correlation ($r = 0.667$) with an $r^2 = 0.445$ (Figure 4h). The equation of the regression analysis is $y = 0.3982 x + 7.7096$.

From the FTIR data of the control and ribose-treated samples, other FTIR parameters were evaluated and are shown in Table 1. Here, the matrix maturity ratio was significantly higher in the ribose-treated samples in comparison to the control ($p < 0.05$). However, the mineral-to-matrix ratio, carbonate-to-phosphate ratio, and 1661/1678 cm^{-1} enzymatic crosslink ratio did not reveal any differences between the control and ribated groups (Table 1).

3.3 Investigation of non-enzymatic cross-links with FTIR: osteoporotic and bisphosphonate-treated bone

FTIR imaging was performed on a set of human biopsies from the iliac crest of treatment-naïve osteoporosis cases and bisphosphonate-treated osteoporosis cases (third generation bisphosphonate). The NE-xLR calculated from the 1678 /1692 cm^{-1} subbands was not significantly different before and after bisphosphonate administration at a dosage recommended by the manufacturer (osteoporotic: NE-xLR = 10.01 ± 2.21, post bisphosphonate treatment: NE-xLR = 10.89 ± 1.36). Fluorescence microscopy also did not find a significant difference in the peak fluorescence between the osteoporotic and bisphosphonate-treated osteoporotic bone (osteoporotic: peak fluorescence = 53.37 ± 15.24, post bisphosphonate treatment: peak fluorescence = 56.19 ± 12.77). Additionally, the matrix maturity rate was calculated for this cohort but did not reveal any significant differences (osteoporotic: matrix maturity = 10.58 ± 2.71, post bisphosphonate treatment: matrix maturity = 11.05 ± 2.25).

While FTIR imaging did not find a difference in the NE-xLR between the osteoporosis and bisphosphonate-treated osteoporosis cases, NE-xLR in the osteoporosis cases had a significantly higher value than the young control-treated samples (young control-treated: NE-xLR = 8.79 ± 1.65, osteoporosis: NE-xLR = 10.01 ± 2.21, $p < 0.05$) and a significantly lower value than the young ribose-treated samples (young ribose-treated: 11.95 ± 1.55, osteoporosis: NE-xLR = 10.01 ± 2.21, $p < 0.05$). Similarly, fluorescence microscopy confirmed a higher peak fluorescence in the osteoporotic bone in comparison to the young bone (osteoporotic bone: peak fluorescence = 53.37 ± 15.24, young control treated: peak-fluorescence = 24.08 ± 5.54, $p < 0.05$, Tukey-B as post-hoc test) and a higher peak fluorescence in the young ribose-treated bone samples compared to the osteoporosis and bisphosphonate-treated groups (osteoporotic bone: peak fluorescence = 53.37 ± 15.24, post bisphosphonate treatment: peak fluorescence = 56.19 ± 12.77, young ribose-treated: peak-fluorescence = 113.13 ± 7.26, $p < 0.05$, Tukey-B as post-hoc test).

4 Discussion

The characterization of non-enzymatic cross-links is critical to investigations of bone quality in diabetes mellitus and skeletal aging, where the accumulation of non-enzymatic cross-links has been related to detrimental effects on the mechanical integrity and fracture resistance of bone tissue. Further developments to understand fracture risk due to bone disease require a greater understanding of the role of cross-links. Here, spatially resolved FTIR imaging was used to analyze cross-linking in human bone due to an *in vitro* ribation treatment as well as before and after bisphosphonate treatment in osteoporosis cases. FTIR imaging of non-enzymatic cross-links provides a novel measure of bone quality at a high spatial resolution

and can be used in conjunction with numerous previously established bone quality parameters (*i.e.,* mineralization distribution, mineral crystal size, enzymatic cross-link content, and mineral age).

Here, a FTIR parameter describing the effect of changes in non-enzymatic cross-links was found within the amide I band of human bone's FTIR spectrum. Non-enzymatic crosslinks, which are common in bone and are known to be induced by ribation [41], absorb infrared radiation in the regions between 1770 – 1570 cm^{-1} and 1250 – 1100 cm^{-1} (Figure 1b). These peaks in the FTIR spectra of non-enzymatic cross-links overlap with the amide I and phosphate peaks in the FTIR spectra of human bone (see Figure 1a,b). Thus, here, we chose to analyze the amide I peak for non-enzymatic cross-links because 1) the phosphate peak has a strong signal mostly associated with mineralization and 2) the amide I peak incorporates a signal from collagen type I, which is also directly affected by the presence of non-enzymatic cross-links. Indeed, non-enzymatic crosslinks will influence the vibration of the amide I peak *e.g.* by limiting vibrations or creating new vibrations due to chemical bonds. The investigation of the single amide I peak is appropriate because this peak does not have a contribution from the mineral phase contrary to the amide II peak, which overlaps with mineral contributions (see Figure 1 and [36]).

The subbands used to calculate the NE-xLR are located within the amide I absorption peak of human bone, which has been associated with the structure of collagen [25,28,34,35,37,42,43]. Thus, it is reasonable to observe changes in this region not only from non-enzymatic cross-links but also from changes in the molecular vibrations of the collagen molecules due to new non-enzymatic cross-links between collagen molecules and fibrils, which would change the molecular vibrations. The 1678 cm^{-1} absorption in the FTIR spectrum of bone is associated with the β-turn conformation of collagen. This conformation is important for the accessibility of lysine [44], which is a binding residue required for cross-links between two collagen molecules [15]. Thus, while the area ratio of the 1678 / 1692 cm^{-1} subbands increases with the increase in non-enzymatic cross-links, it is unclear whether the change in the ratio is due to the molecular vibrations of non-enzymatic crosslinks or whether it signifies structural changes in the higher level features of the collagen molecules. In this study, the amount of non-enzymatic cross-links in the ribose-treated group was the only change in the structure in comparison to the control treatment. *Thus, we define the NE-xLR to be a measure of collagen quality associated with the non-enzymatic cross-link content.*

The NE-xLR was found to have a 35% higher value in the ribose-treated samples vs. the young cases undergoing control treatment (Figure 3a). The *in vitro* ribose treatment is a well-known method used to increase the non-enzymatic cross-link content in bone with respect to a control treatment. Thus, with the ribation method, the effects of non-enzymatic cross-links can be isolated because this is the only major change in the bone structure, which was confirmed by measuring other FTIR parameters that characterize collagen content, enzymatic cross-links and mineralization (Table 1). In particular, the enzymatic cross-link ratio, which was recently reported by Paschalis et al., linked the 1678 cm^{-1} peak in combination with the 1660 cm^{-1} peak to enzymatic crosslinks [38]. As expected, in this study with the *in vitro* ribation treatment, no significant change was detected in the 1661 /

1678 cm^{-1} ratio because no enzymes were active in the *ex vivo* samples to induce enzymatic cross-links (Table 1). The only significant change was found in the matrix maturity, which could also be measuring similar changes in the collagen environment as the NE-xLR.

In addition to the characteristic browning caused by non-enzymatic cross-links (Figure 2), other well-established methods were used to confirm the increase in non-enzymatic crosslinks in this cohort (see Figure 4), where significant correlations were found between the NE-xLR and the UPLC, fluorescence imaging and fluorometric assay. The main reason for differences between the methods is explained by how the different techniques probe and reflect unique aspects/representations of the non-enzymatic crosslinks. FTIR leverages the vibrations of molecules while the fluorescence approaches use the fluorometric characteristics of molecules. This means an absence of a defined molecule at a certain wavelength will make the fluorescence disappear. However, in FTIR, the absence of non-enzymatic crosslinks will just change the peak contribution to the whole spectrum but will not cause the peak to vanish because the amide I peak is linked to vibrations on the collagen itself. Changes in the structure (due to crosslinking) will increase or decrease the vibrational contribution. Given that these methods probe unique and disparate physical molecular characteristics, the correlations between the NE-xLR and the UPLC, fluorescence micrsocopy and the fluorometric assay are particular encouraging confirmations of the increase of nonenzymatic crosslinking. Furthermore, these results suggest that the peak area ratio of the 1678 / 1692 cm^{-1} subbands may be a good independent measurement of crosslinks that correlate with the pentosidine and total fluorescent non-enzymatic cross-link content.

The NE-xLR was additionally measured on trabecular bone from human iliac crest biopsies taken from osteoporotic individuals before and after bisphosphonate treatment. Here, the NE-xLR was not significantly different before and after bisphosphonate treatment. These FTIR results are supported by fluorescence microscopy, which also did not find a difference in the peak fluorescence from non-enzymatic cross-links. The increase in non-enzymatic cross-links with bisphosphonate treatment is a controversial subject. Previously, high levels of non-enzymatic cross-links were found in bisphosphonate-treated canine tissue; however, the dose of bisphosphonate was higher than the clinical recommendations and an osteoporotic model was not included in the canine study design [20]. Further analysis on the mineralization kinetics would be required here to assess the present bone turnover state before making further conclusions.

The NE-xLR and the fluorescence microscopy for the bisphosphonate-treated samples did show significantly higher values than the young control-treated samples. The comparison of osteoporotic and bisphosphonate-treated bone to young and D-ribose treated bone highlights an expected gradient of non-enzymatic crosslinks in the four tested groups. The ribose-treated, osteoporotic and bisphosphonate treated samples exhibit higher NE-xLR than young bone. These results of the NE-xLR and the fluorescence microscopy fit with the expectation that young bone has the lowest amount of non-enzymatic cross-links and osteoporotic as well as ribose-treated (i.e., artificially aged bone) samples have a high amount of non-enzymatic cross-links.

In terms of the 2D spatial distribution of non-enzymatic cross-links within the bone tissue, the NE-xLR indicates that changes in collagen quality due to non–enzymatic cross-linking is highest in bone with a higher tissue age (Figure 3b, c). In cortical areas, bone remodeling resorbs old bone tissue and creates new tissue in the form of osteons. The osteons are surrounded by interstitial, lamellar bone, which essentially reflect parts of former osteons and therefore predate the current osteons. Thus, some areas of the bone microstructure have an older tissue age (*e.g.,* interstitial tissue) and a younger tissue age (*e.g.,* newly formed osteons) [45]. Similar remodeling processes occur in trabecular bone. Post-translational changes to the collagen in regions with an older tissue age and/or regions with accumulation of dead osteocytes (*i.e.,* micropetrotic bone) could make the older bone tissue more susceptible to changes in the measured collagen quality due to non-enzymatic cross-linking.

The NE-xL ratio represents a new parameter, which is of particular interest for measuring collagen quality in diabetes mellitus. As diabetes mellitus is specifically known to induce non-enzymatic cross-links *in vivo* due to a high presence of glucose [6,13,46], mapping of non-enzymatic cross-links using the NE-xLR will provide additional insight regarding both the amount and spatial distribution of non-enzymatic crosslinks in diseased bone. Such FTIR derived maps with detailed spatial information are capable of highlighting diabetes-induced changes in the collagenous matrix affecting mechanical properties and fracture resistance. Several studies have shown an influence of non-enzymatic cross-links on the biomechanical behavior of bone at increased or decreased sugar levels [13,46–49].

This study investigating non-enzymatic cross-links with FTIR has several limitations. First, a pentosidine standard was used to find an area of interest in the FTIR spectrum; however, pentosidine is not the only non-enzymatic cross-link formed *in vivo*. Nevertheless pentosidine is often used as a measure for collagen crosslinking [6,22] with UPLC but further research should be performed to differentiate other collagen crosslinks. Secondly, there is no possibility to distinguish if there was a higher AGE content before ribation in the interstitial bone or if the induction of non-enzymatic cross-links occurred more extensively in the interstitial bone. Third, the used iliac crest biopsies were not labeled in order to perform bone turnover measurements by dynamic bone histomorphometry.

5 Conclusions

In conclusion, here, we use FTIR imaging to detect changes in collagen quality associated with non-enzymatic collagen cross-links, which play a mechanistic role in generating bone quality and fracture risk in diabetes mellitus, skeletal aging, and other bone diseases. Using FTIR imaging, the changes in collagen quality associated with non-enzymatic collagen cross-links can be measured along with other established bone quality parameters with a high spatial resolution. Here, non-enzymatic collagen cross-links were induced *in vitro* through ribation. FTIR imaging of the control and ribose-treated samples as well as the pre- and post-bisphosphonate-treated samples was used to measure *the non-enzymatic cross-linking ratio (NE-xLR), which is a measure of changes in collagen quality associated with non-enzymatic cross-links, the area ratio of the amide I subbands at 1678 and 1692 cm^{-1}*. This NE-xL ratio, that allows a quantitative spatial assessment of collagen quality associated with non-enzymatic collagen cross-links using FTIR imaging, is highly valuable to

investigations of bone quality in cases of bone diseases, such as diabetes mellitus, skeletal aging and antiresorptive therapies to treat osteoporosis.

Acknowledgments

This project was supported by the German Research Foundation (DFG) under grant no. BU 2562/2-1/3-1 and the Partnership for Innovation, Education and Research (PIER) under grant no PIF-2015-43. Felix Schmidt acknowledges the support of the Joachim Herz Stiftung in cooperation with the PIER initiative of the University of Hamburg and DESY Hamburg. Dr. Zimmermann is supported through a postdoctoral fellowship from the Alexander von Humboldt Foundation. Dr. Vashishth acknowledges the support of NIH grant AG20618.

References

1. Zimmermann EA, Ritchie RO. Bone as a Structural Material. Adv Healthc Mater. 2015; doi: 10.1002/adhm.201500070
2. Carriero A, Zimmermann EA, Paluszny A, Tang SY, Bale H, Busse B, Alliston T, Kazakia G, Ritchie RO, Shefelbine SJ. How Tough Is Brittle Bone? Investigating Osteogenesis Imperfecta in Mouse Bone. J Bone Miner Res. 2014; 29:1392–1401. [PubMed: 24420672]
3. Busse B, Bale HA, Zimmermann EA, Panganiban B, Barth HD, Carriero A, Vettorazzi E, Zustin J, Hahn M, Ager JW, Püschel K, Amling M, Ritchie RO. Vitamin D deficiency induces early signs of aging in human bone, increasing the risk of fracture. Sci Transl Med. 2013; 5:193ra88.
4. Zimmermann EA, Schaible E, Bale H, Barth HD, Tang SY, Reichert P, Busse B, Alliston T, Ager JW, Ritchie RO. Age-related changes in the plasticity and toughness of human cortical bone at multiple length scales. Proc Natl Acad Sci U S A. 2011; 108:14416–14421. [PubMed: 21873221]
5. Karim L, Vashishth D. Heterogeneous glycation of cancellous bone and its association with bone quality and fragility. PloS One. 2012; 7:e35047.doi: 10.1371/journal.pone.0035047 [PubMed: 22514706]
6. Saito M, Marumo K. Collagen cross-links as a determinant of bone quality: a possible explanation for bone fragility in aging, osteoporosis, and diabetes mellitus. Osteoporos Int J Establ Result Coop Eur Found Osteoporos Natl Osteoporos Found USA. 2010; 21:195–214.
7. Vashishth D, Gibson GJ, Khoury JI, Schaffler MB, Kimura J, Fyhrie DP. Influence of nonenzymatic glycation on biomechanical properties of cortical bone. Bone. 2001; 28:195–201. [PubMed: 11182378]
8. Weiner S, Wagner HD. The Material Bone: Structure-Mechanical Function Relations. Annu Rev Mater Sci. 1998; 28:271–298.
9. Bailey AJ. Molecular mechanisms of ageing in connective tissues. Mech Ageing Dev. 2001; 122:735–755. [PubMed: 11322995]
10. Avery NC, Bailey AJ. The effects of the Maillard reaction on the physical properties and cell interactions of collagen. Pathol Biol (Paris). 2006; 54:387–395. [PubMed: 16962252]
11. Sell DR, Nagaraj RH, Grandhee SK, Odetti P, Lapolla A, Fogarty J, Monnier VM. Pentosidine: a molecular marker for the cumulative damage to proteins indiabetes, aging, and uremia. Diabetes Metab Rev. 1991; 7:239–251. [PubMed: 1813279]
12. Rubin MR, Paschalis EP, Poundarik A, Sroga GE, McMahon DJ, Gamsjaeger S, Klaushofer K, Vashishth D. Advanced Glycation Endproducts and Bone Material Properties in Type 1 Diabetic Mice. PloS One. 2016; 11:e0154700.doi: 10.1371/journal.pone.0154700 [PubMed: 27140650]
13. Saito M, Kida Y, Kato S, Marumo K. Diabetes, collagen, and bone quality. Curr Osteoporos Rep. 2014; 12:181–188. [PubMed: 24623537]
14. Siegmund T, Allen MR, Burr DB. Failure of mineralized collagen fibrils: modeling the role of collagen cross-linking. J Biomech. 2008; 41:1427–1435. [PubMed: 18406410]
15. Garnero P. The contribution of collagen crosslinks to bone strength. BoneKEy Rep. 2012; 1:182. [PubMed: 24363926]
16. Barth HD, Zimmermann EA, Schaible E, Tang SY, Alliston T, Ritchie RO. Characterization of the effects of x-ray irradiation on the hierarchical structure and mechanical properties of human cortical bone. Biomaterials. 2011; 32:8892–8904. [PubMed: 21885114]

17. Saito M, Fujii K, Soshi S, Tanaka T. Reductions in degree of mineralization and enzymatic collagen cross-links and increases in glycation-induced pentosidine in the femoral neck cortex in cases of femoral neck fracture. Osteoporos Int J Establ Result Coop Eur Found Osteoporos Natl Osteoporos Found USA. 2006; 17:986–995. DOI: 10.1007/s00198-006-0087-0

18. Saito M, Marumo K, Kida Y, Ushiku C, Kato S, Takao-Kawabata R, Kuroda T. Changes in the contents of enzymatic immature, mature, and non-enzymatic senescent cross-links of collagen after once-weekly treatment with human parathyroid hormone (1-34) for 18 months contribute to improvement of bone strength in ovariectomized monkeys. Osteoporos Int J Establ Result Coop Eur Found Osteoporos Natl Osteoporos Found USA. 2011; 22:2373–2383. DOI: 10.1007/s00198-010-1454-4

19. Willett TL, Pasquale J, Grynpas MD. Collagen Modifications in Postmenopausal Osteoporosis: Advanced Glycation Endproducts May Affect Bone Volume, Structure and Quality. Curr Osteoporos Rep. 2014; 12:329–337. DOI: 10.1007/s11914-014-0214-3 [PubMed: 24880722]

20. Allen MR, Gineyts E, Leeming DJ, Burr DB, Delmas PD. Bisphosphonates alter trabecular bone collagen cross-linking and isomerization in beagle dog vertebra. Osteoporos Int J Establ Result Coop Eur Found Osteoporos Natl Osteoporos Found USA. 2008; 19:329–337.

21. Tang SY, Allen MR, Phipps R, Burr DB, Vashishth D. Changes in non-enzymatic glycation and its association with altered mechanical properties following 1-year treatment with risedronate or alendronate. Osteoporos Int J Establ Result Coop Eur Found Osteoporos Natl Osteoporos Found USA. 2009; 20:887–894.

22. Viguet-Carrin S, Roux JP, Arlot ME, Merabet Z, Leeming DJ, Byrjalsen I, Delmas PD, Bouxsein ML. Contribution of the advanced glycation end product pentosidine and of maturation of type I collagen to compressive biomechanical properties of human lumbar vertebrae. Bone. 2006; 39:1073–1079. [PubMed: 16829221]

23. Sroga GE, Vashishth D. UPLC methodology for identification and quantitation of naturally fluorescent crosslinks in proteins: a study of bone collagen. J Chromatogr B Analyt Technol Biomed Life Sci. 2011; 879:379–385. DOI: 10.1016/j.jchromb.2010.12.024

24. Sroga GE, Siddula A, Vashishth D. Glycation of human cortical and cancellous bone captures differences in the formation of Maillard reaction products between glucose and ribose. PloS One. 2015; 10:e0117240.doi: 10.1371/journal.pone.0117240 [PubMed: 25679213]

25. Paschalis EP, Mendelsohn R, Boskey AL. Infrared assessment of bone quality: a review. Clin Orthop. 2011; 469:2170–2178. [PubMed: 21210314]

26. Gong B, Mandair GS, Wehrli FW, Morris MD. Novel assessment tools for osteoporosis diagnosis and treatment. Curr Osteoporos Rep. 2014; 12:357–365. [PubMed: 24879507]

27. Camacho NP, Landis WJ, Boskey AL. Mineral changes in a mouse model of osteogenesis imperfecta detected by Fourier transform infrared microscopy. Connect Tissue Res. 1996; 35:259–265. [PubMed: 9084664]

28. Farlay D, Duclos ME, Gineyts E, Bertholon C, Viguet-Carrin S, Nallala J, Sockalingum GD, Bertrand D, Roger T, Hartmann DJ, Chapurlat R, Boivin G. The ratio 1660/1690 cm(-1) measured by infrared microspectroscopy is not specific of enzymatic collagen cross-links in bone tissue. PloS One. 2011; 6:e28736. [PubMed: 22194900]

29. Boskey A, Pleshko Camacho N. FT-IR imaging of native and tissue-engineered bone and cartilage. Biomaterials. 2007; 28:2465–2478. [PubMed: 17175021]

30. Guilbert M, Said G, Happillon T, Untereiner V, Garnotel R, Jeannesson P, Sockalingum GD. Probing non-enzymatic glycation of type I collagen: a novel approach using Raman and infrared biophotonic methods. Biochim Biophys Acta. 2013; 1830:3525–3531. DOI: 10.1016/j.bbagen.2013.01.016 [PubMed: 23380466]

31. Roy R, Boskey A, Bonassar LJ. Processing of type I collagen gels using nonenzymatic glycation. J Biomed Mater Res A. 2010; 93:843–851. DOI: 10.1002/jbm.a.32231 [PubMed: 19658163]

32. Spalazzi JP, Boskey AL, Pleshko N, Lu HH. Quantitative Mapping of Matrix Content and Distribution across the Ligament-to-Bone Insertion. PLoS ONE. 2013; 8doi: 10.1371/journal.pone.0074349

33. Pleshko NL, Boskey AL, Mendelsohn R. An FT-IR microscopic investigation of the effects of tissue preservation on bone. Calcif Tissue Int. 1992; 51:72–77. [PubMed: 1393781]

34. Camacho NP, West P, Torzilli PA, Mendelsohn R. FTIR microscopic imaging of collagen and proteoglycan in bovine cartilage. Biopolymers. 2001; 62:1–8. [PubMed: 11135186]
35. Movasaghi Z, Rehman S, ur Rehman DI. Fourier Transform Infrared (FTIR) Spectroscopy of Biological Tissues. Appl Spectrosc Rev. 2008; 43:134–179.
36. Figueiredo, MM., Martins, AG., Gamelas, JAF. [accessed December 28, 2015] Characterization of bone and bone-based graft materials using FTIR spectroscopy. INTECH Open Access Publisher. 2012. http://cdn.intechopen.com/pdfs/36055.pdf
37. Bryan MA, Brauner JW, Anderle G, Flach CR, Brodsky B, Mendelsohn R. FTIR studies of collagen model peptides: complementary experimental and simulation approaches to conformation and unfolding. J Am Chem Soc. 2007; 129:7877–7884. [PubMed: 17550251]
38. Paschalis EP, Gamsjaeger S, Tatakis DN, Hassler N, Robins SP, Klaushofer K. Fourier transform Infrared spectroscopic characterization of mineralizing type I collagen enzymatic trivalent cross-links. Calcif Tissue Int. 2015; 96:18–29. DOI: 10.1007/s00223-014-9933-9 [PubMed: 25424977]
39. Woessner JF. The determination of hydroxyproline in tissue and protein samples containing small proportions of this imino acid. Arch Biochem Biophys. 1961; 93:440–447. [PubMed: 13786180]
40. Busse B, Jobke B, Seitz S, Hahn M, Zustin J, Duda GN, Semler J, Amling M. The degree of superimposed antiresorptive effects on bone quality: Analyses of histomorphometric indices and mineral composition in face of the T-score on 15 paired iliac crest biopsies underlying long-term bisphosphonate treatment. Bone. 2009; 44:S426.
41. Grandhee SK, Monnier VM. Mechanism of formation of the Maillard protein crosslink pentosidine. Glucose, fructose, and ascorbate as pentosidine precursors. J Biol Chem. 1991; 266:11649–11653. [PubMed: 1904866]
42. Khanarian NT, Boushell MK, Spalazzi JP, Pleshko N, Boskey AL, Lu HH. FTIR-I compositional mapping of the cartilage-to-bone interface as a function of tissue region and age. J Bone Miner Res Off J Am Soc Bone Miner Res. 2014; 29:2643–2652.
43. Kong J, Yu S. Fourier transform infrared spectroscopic analysis of protein secondary structures. Acta Biochim Biophys Sin. 2007; 39:549–559. [PubMed: 17687489]
44. Rabotyagova OS, Cebe P, Kaplan DL. Collagen Structural Hierarchy and Susceptibility to Degradation by Ultraviolet Radiation. Mater Sci Eng C Mater Biol Appl. 2008; 28:1420–1429. [PubMed: 22199459]
45. Sroga GE, Karim L, Colón W, Vashishth D. Biochemical characterization of major bone-matrix proteins using nanoscale-size bone samples and proteomics methodology. Mol Cell Proteomics MCP. 2011; 10 M110.006718. doi: 10.1074/mcp.M110.006718
46. Campbell GM, Tiwari S, Hofbauer C, Picke AK, Rauner M, Huber G, Peña JA, Damm T, Barkmann R, Morlock MM, Hofbauer LC, Glüer CC. Effects of parathyroid hormone on cortical porosity, non-enzymatic glycation and bone tissue mechanics in rats with type 2 diabetes mellitus. Bone. 2016; 82:116–121. DOI: 10.1016/j.bone.2015.04.049 [PubMed: 25952971]
47. Hamann C, Picke AK, Campbell GM, Balyura M, Rauner M, Bernhardt R, Huber G, Morlock MM, Günther KP, Bornstein SR, Glüer CC, Ludwig B, Hofbauer LC. Effects of Parathyroid Hormone on Bone Mass, Bone Strength, and Bone Regeneration in Male Rats With Type 2 Diabetes Mellitus. Endocrinology. 2014; 155:1197–1206. DOI: 10.1210/en.2013-1960 [PubMed: 24467747]
48. Picke AK, Gordaliza Alaguero I, Campbell GM, Glüer CC, Salbach-Hirsch J, Rauner M, Hofbauer LC, Hofbauer C. Bone defect regeneration and cortical bone parameters of type 2 diabetic rats are improved by insulin therapy. Bone. 2016; 82:108–115. DOI: 10.1016/j.bone.2015.06.001 [PubMed: 26055107]
49. Poundarik AA, Wu PC, Evis Z, Sroga GE, Ural A, Rubin M, Vashishth D. A direct role of collagen glycation in bone fracture. J Mech Behav Biomed Mater. 2015; 52:120–130. DOI: 10.1016/j.jmbbm.2015.08.012 [PubMed: 26530231]
50. Stuart, BH. Infrared Spectroscopy: Fundamentals and Applications. 1. Wiley; 2007.
51. Pavia, DL., L, Gary M., Kriz, George S. Introduction to Spectroscopy : A Guide for Students of Organic Chemistry. W B Saunders Company; 1979.

Highlights

- High-resolution FTIR mapping allows quantitative spatial assessment of collagen quality associated with non-enzymatic collagen cross-link alterations (e.g. diabetes, *etc.*)
- Area ratio of the Amide I subbands at 1678 and 1692 cm^{-1} is sensitive to changes in collagen quality associated with non-enzymatic collagen cross-links in bone
- Young individuals and young bone packets show the lowest amount of non-enzymatic cross-links
- Osteoporotic and ribose-treated (i.e., artificially aged bone) samples reveal high amount of non-enzymatic cross-links
- Changes in non-enzymatic cross-links detected with FTIR are in line with established fluorometric assays, fluorescence microscopy and ultra-high pressure liquid chromatography

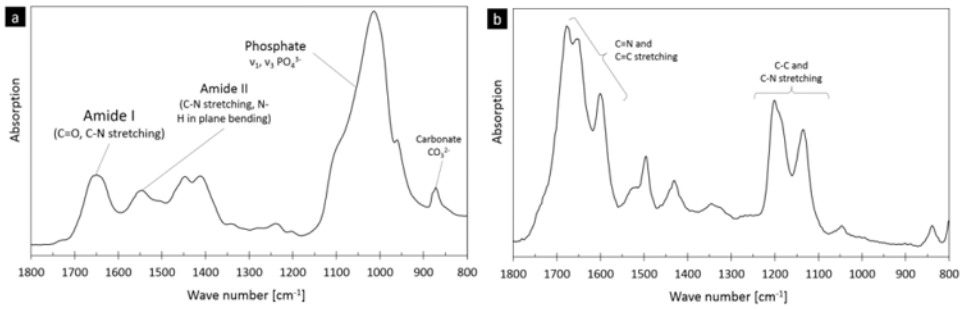

Figure 1. FTIR spectra for human bone and the non-enzymatic cross-link, pentosidine

Fourier transform infrared (FTIR) spectroscopy is able to detect chemical bonding in materials. Here, representative spectra from (a) human bone and (b) the non-enzymatic crosslink, pentosidine, are shown. The main vibrations of pentosidine refer to C=N and C=C stretching as well as C-C and C-N stretching. These non-enzymatic cross-link vibrational regions are within human bone's amide I peak (C=O and C-N stretching, 1770-1570 cm^{-1}) and phosphate peak (C-C and C-N stretching, 1250-1100 cm^{-1}), respectively [50,51].

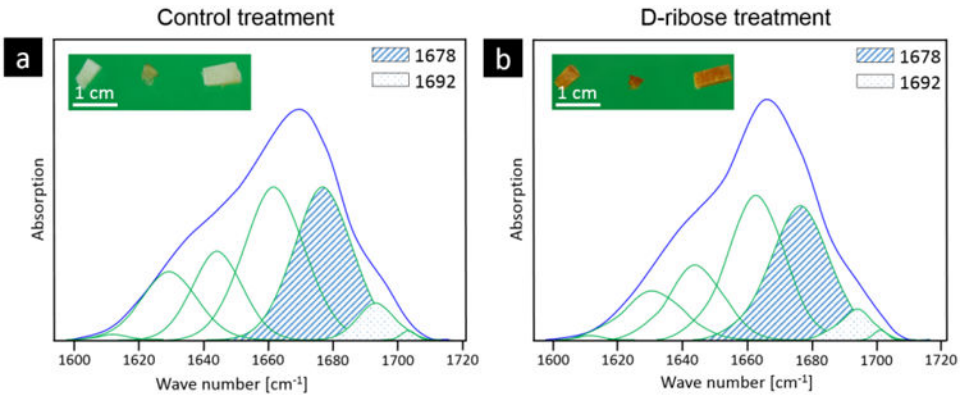

Figure 2. Peak fitting of amide I band

The subbands of the amide I band were peak fit with seven Gaussian curves at 1610, 1630, 1645, 1660, 1678, 1692 and 1702 cm^{-1} for each spectra from the a) control and b) ribated treatment groups. The bone from the (a) control treatment has a characteristic white color, while the (b) ribose-treated samples have a yellow-orange color, which is characteristic of a higher non-enzymatic cross-link content. Based on the subband analysis, an area ratio of 1678 (hatched area) and 1692 (dotted area) cm^{-1} subbands was calculated.

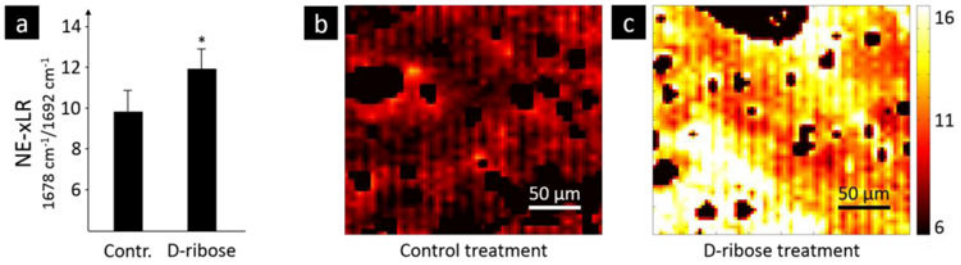

Figure 3. FTIR imaging: Non-enzymatic cross-link ratio in ribated bone

Samples of human cortical bone from the mid-diaphysis of the femur were subjected to an *in vitro* control or ribation treatment, the latter increases the non-enzymatic cross-links content. FTIR spectra were obtained over a 250 × 250 μm^2 area of bone at a 6.25-µm step size and the non-enzymatic cross-link ratio (NE-xLR), which is the area ratio of the amide-I subbands at 1678 and 1692 cm^{-1}, was calculated for each spectra. a) The average NE-xLR ratio was 35% higher in the ribation group in comparison to the control group ($p < 0.005$). The NE-xLR distribution can be seen in the FTIR images of b) control and c) ribated samples. Clearly an osteon with a low level of NE-xLR is to be seen in the upper left corner in b) and in c) a slightly diagonal cut osteon is going through the whole image from left upper corner to right lower corner with higher levels of the NE-xLR in the interstitial area (lower left corner).

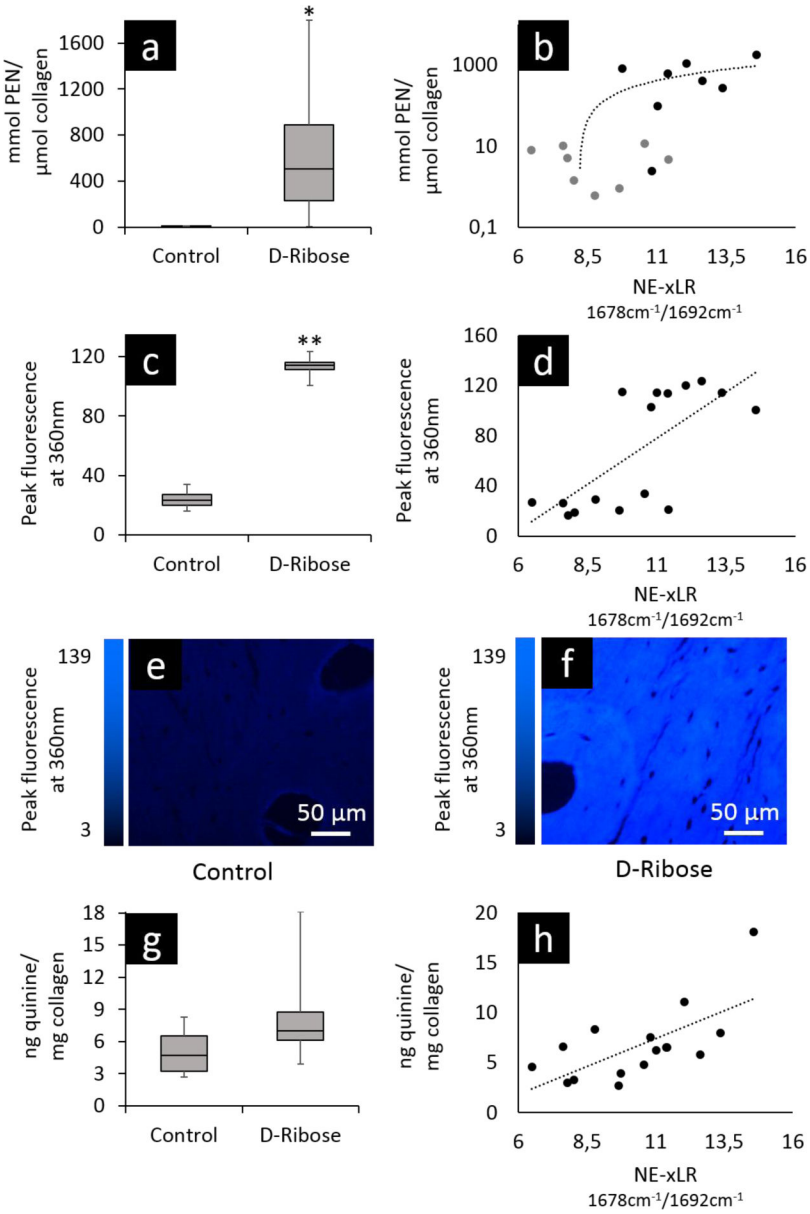

Figure 4. Confirmation of non-enzymatic cross-link content after control and ribose treatments

Following an *in vitro* control or ribose treatment, human cortical bone samples were analyzed with three well-established methods to measure non-enzymatic cross-links to confirm that the ribose treatment increased the non-enzymatic cross-link content in relation to the control treatment. First, *ultra-high pressure liquid chromatography* (UPLC) was used to measure the specific content of the non-enzymatic cross-link, pentosidine. **(a)** The pentosidine content (nmol PEN / µmol Col) is 120 times greater in the ribose-treated group vs control ($p < 0.01$). **(b)** The UPLC data (logarithmic scale) correlates significantly with the results of the NE-xLR measured with FTIR imaging ($p < 0.01$). **(c)** *Fluorescence microscopy,* which measures the content of non-enzymatic cross-links, also confirms a 470% higher peak fluorescence in the ribated group ($p < 0.00001$) and **(d)** shows a significant correlation with the FTIR imaging results ($p < 0.005$). Indeed, representative images from fluorescence

microscopy show the dramatic differences in cross-link fluorescence between the **(e)** control and **(f)** ribated samples. **(g)** Lastly, a *fluorometric assay* was performed, which measures non-enzymatic cross-link content. While these data were not significant between the control and ribated samples, **(h)** the correlation between the results of the fluorometric assay and the NE-xLR were significant ($p < 0.01$).

Table 1

Additional parameters calculated from the FTIR spectra of the control and ribated groups. Significant differences were not found in the mineral-associated parameters (Mineral-to-Matrix and Carbonate-to-Phosphate ratios) nor in the enzymatic cross-link ratio (1661/1678 cm^{-1}). However, the ribose-treated samples did have a significantly higher matrix maturity ratio, as non-enzymatic crosslinking are known to alter the bone matrix. Thus, ribose treatment had no influence on the mineral and matrix components in bone apart from increasing the non-enzymatic cross-link content. Mineral parameters were measured using a universal-ATR-crystal.

	Mineral/Matrix	Carbonate/Phosphate	Matrix maturity	Enzymatic crosslink ratio 1661/1678 cm^{-1}
Control	3.66 ± 0.3	0.0125 ± 0.005	9.66 ± 1.83	1.36± 0.18
D-ribose treated	3.55 ± 0.31	0.0138 ± 0.0048	12.2 ± 1.49	1.27± 0.16
p-value	p = 0.48	p = 0.62	p = 0.013	p = 0.37